Real-Time Compensation in Organic Light-Emitting Diode Television Displays Using Current Sensing Method With Charge Integrators

Myung Gi Lim and Seung-Woo Lee, *Senior Member, IEEE*

***Abstract*— This paper proposes a novel method for sensing and compensating for the characteristics of thin-film transistors (TFTs) in organic light-emitting diode (OLED) television (TV) displays. The proposed method uses a charge integrator (CI) to sense the TFT currents and calculates the TFT threshold voltage (V_{TH}) and transconductance parameter (K) using the two different sensed currents. The sensing of the two different currents can be performed within 300 μs, which is the vertical blank time for an ultra-high-definition resolution with a refresh rate of 120 Hz, enabling real-time compensation. A new measurement method of all feedback capacitors (C_{FB} s) of CIs is proposed to overcome the variation of C_{FB}. The proposed sensing circuit uses differential sensing and auto-zero methods to provide high panel noise immunity and accurate sensing. The performance of the compensation was estimated using Smart-SPICE (Simulation Program with Integrated Circuit Emphasis) simulation under the conditions of ±0.5 V and ±10 % variations in V_{TH} and K, respectively. The simulation demonstrated that the current deviation decreased from a maximum of 98.8 % before compensation to 2.3 % after compensation. The compensation performance of the proposed method was verified using a 13.7-inch active-matrix OLED (AMOLED) panel with a resolution of 960 × 540. The results showed that the current deviation of the 13.7-inch AMOLED panel decreased from 40.4 % before compensation to 2.7 % after compensation. The proposed method offers a more accurate and faster compensation solution for high-resolution and large-sized OLED TV displays compared to conventional methods.**

***Index Terms*— Active-matrix organic light-emitting diode (AMOLED), charge integrator (CI), external compensation, OLED television (TV), real-time, thin-film transistors (TFTs), threshold voltage (V_{TH}).**

I. Introduction

TODAY, flat panel displays are widely used in various applications and the demand for high-performance displays with large sizes and high resolutions is increasing [1], [2], [3]. In the past, liquid crystal displays (LCDs) dominated the flat panel display market, but organic light-emitting diode (OLED) displays are gaining market share in the mobile and television (TV) display market. OLED displays are attracting attention for their outstanding advantages, such as a wide viewing angle, high contrast ratio, and short response time [4], [5], [6]. Additionally, OLED technology is seen as a key technology for future displays, such as transparent and flexible displays [7], [8]. Because OLEDs are current-driven devices, a thin film transistor (TFT) is responsible for supplying the current to the OLED. The OLED luminance is proportional to the current supplied, so the quality of the display directly depends on the characteristics of the TFT. The drain-to-source current (I_{DS}) of the TFT is expressed by,

$$I_{DS} = K\,(V_{GS} - V_{TH})^2 \tag{1}$$

$$K = \frac{1}{2}\mu C_{ox}\frac{W}{L} \tag{2}$$

where V_{TH} is the threshold voltage, and K is the transconductance parameter that includes the mobility (μ), the ratio of width to length (W/L) of the TFT channel, and the gate capacitance per unit area (C_{ox}). The I_{DS} of a TFT at the same gate-source voltage (V_{GS}) depends on the deviation of two key parameters, K and V_{TH}. K and V_{TH} of all TFTs are not identical because of process variations. Additionally, K and V_{TH} may vary due to electrical and thermal stresses during operation [9], [10], [11]. The non-uniform TFT characteristics and unreliable performance degradation result in non-uniform luminance across the display screen. To address this issue, it is necessary to compensate for the TFT characteristics so that the same current is supplied for the same image data.

There are two main methods to compensate for TFT characteristics: an internal compensation method and an external compensation method. The internal compensation method utilizes an in-pixel compensation circuit [12], [13], [14], whereas the external compensation method uses circuits outside the panel [15], [16], [17], [18]. This results in simpler pixel circuits in the external compensation method. However, the internal compensation method reduces the aperture ratio as it requires a large number of TFTs and capacitors in a pixel [19]. To increase the aperture ratio, external compensation is used in large-sized OLED TV panels [20].

In the case of external compensation, the TFT characteristics are sensed by an external sensing circuit. The deviation is compensated for by adding it to the data voltage (V_{DATA}) after the TFT characteristics have been calculated based on the sensed data [21], [22].

Manuscript received 19 April 2023; revised 21 July 2023 and 23 August 2023; accepted 18 September 2023. Date of publication 5 October 2023; date of current version 18 December 2023. This work was supported by LG Display Company Ltd. This article was recommended by Associate Editor H. Dinc. *(Corresponding author: Seung-Woo Lee.)*

The authors are with the Department of Information Display, Kyung Hee University, Dongdaemun-gu, Seoul 02447, Republic of Korea (e-mail: seungwoolee@khu.ac.kr).

Color versions of one or more figures in this article are available at https://doi.org/10.1109/TCSI.2023.3318247.

Digital Object Identifier 10.1109/TCSI.2023.3318247

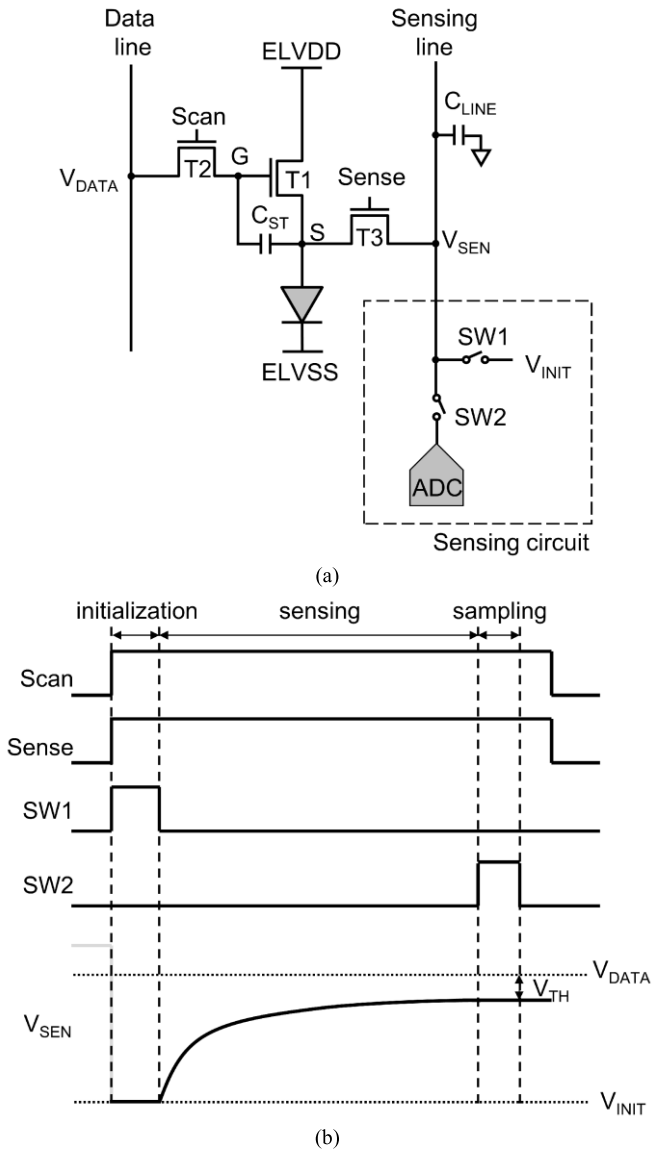

Fig. 1. (a) 3T1C OLED pixel and simplified block diagram of the conventional external sensing circuit. (b) Timing diagrams of the voltage waveforms for V_{TH} sensing.

As shown in Fig. 1(a), the conventional external compensation method has a pixel structure that consists of three TFTs and one capacitor (3T1C) [23]. The driver IC includes an analog-to-digital converter (ADC) and switches that comprise the sensing circuit. Fig. 1(b) shows the voltage change of the sensing line (V_{SEN}) and the timing diagram of the control signals for V_{TH} sensing. The V_{TH} sensing procedure consists of three steps: initialization, sensing, and sampling. During initialization, Scan, Sense, and SW1 signals are set to a high level. Then, T2 and T3 are turned on, causing the V_{GS} of T1 to become $V_{DATA} - V_{INIT}$. During sensing, the Scan and Sense signals remain high, and SW1 signal is set to a low level. The gate node of T1 is fixed to V_{DATA}, and its source node becomes floating. As the I_{DS} of T1 charges the capacitive load of the sensing line (C_{LINE}), the source node voltage (V_S) increases. V_S continues to increase until the V_{GS} of T1 reaches V_{TH}, causing T1 to turn off. Thus, V_{DATA} − (the saturated V_S) becomes the V_{TH} of T1. During sampling, SW2 signal is set to a high level. The ADC then converts the saturated V_S value to its corresponding digital value. The compensation data value can be calculated easily using the digital value and V_{DATA}.

It takes more than tens of milliseconds to complete the three steps [24], [25]. Thus, it takes more than tens of seconds to detect the exact V_{TH} values of all the driving TFTs on a panel. Furthermore, larger or higher-resolution panels require more sensing time. This is because C_{LINE} is charged by the I_{DS} of T1 during V_{TH} sensing, and larger C_{LINE} requires longer sensing times [26]. As a result, real-time compensation for V_{TH} is not possible using the conventional method during operation, but it can be done just before power-off. On the other hand, mobile OLED displays that adopt the internal compensation method perform the V_{TH} compensation in real-time, ensuring the image quality is maintained regardless of operation time. However, the image quality of OLED TVs can degrade over time as the operation continues without being powered off.

This paper presents a novel external compensation method that can be performed within a vertical blank time by sensing TFT characteristics in a significantly shorter time than the conventional method. Previous studies on real-time TFT compensation either require more time than the vertical blank time of the latest display products, or they do not consider variations in K [24], [25], [26], [27].

The proposed method maintains uniformity in TFT current by periodically sensing and compensating during the vertical blank time. To accomplish this, we propose a method for sensing TFT currents using a charge integrator (CI) and a method for calculating V_{TH} and K values using two sensed current values. Although CIs are used as sensors in various applications, there has been no research on sensing and compensating for TFT characteristics in OLED TV displays. Additionally, the proposed method uses a measurement of all feedback capacitors (C_{FB}s), differential sensing, and auto-zero methods to remove sensing noise and errors, respectively. The effectiveness of the proposed compensation method was verified on a 13.7-inch active-matrix OLED (AMOLED) panel.

II. Proposed Sensing and Compensation Method

Fig. 2(a) shows the pixel structure and the novel sensing circuit proposed in this paper. The pixel structure is the 3T1C, which is the same as that of the conventional external compensation method. However, the sensing circuit includes an added component, a CI.

The CI measures the T1 current in a much shorter time, as the current flows through the smaller C_{FB} included in the CI. This results in a quicker measurement of the current than the conventional method where the ADC measures the voltage caused by the current flowing through the larger C_{LINE}. As a result, the proposed method provides far shorter sensing times than the conventional method. In addition, it is not affected by differences in C_{LINE} with panel size and resolution. Fig. 2(b) shows a circuit diagram of a CI amplifier. Fig. 2(c) shows the waveforms of the control signals and the voltage of the sensing line. The operation of the proposed method consists of three steps, similar to the conventional method: initialization, sensing, and sampling. During initialization, Scan, Sense,

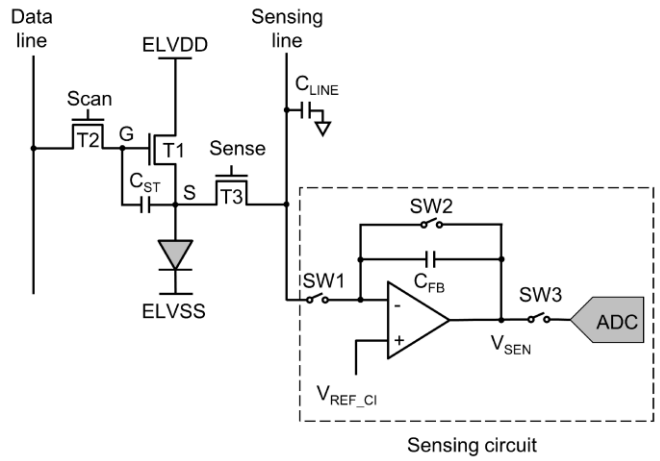

(a)

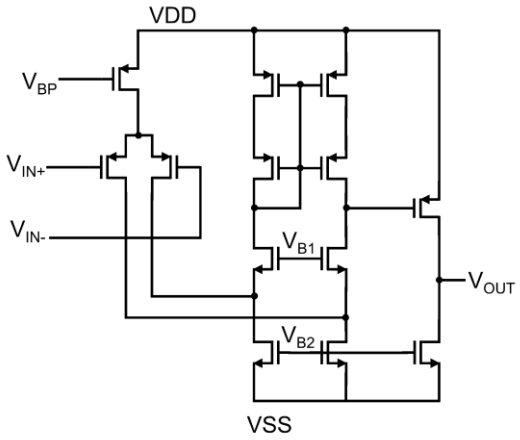

(b)

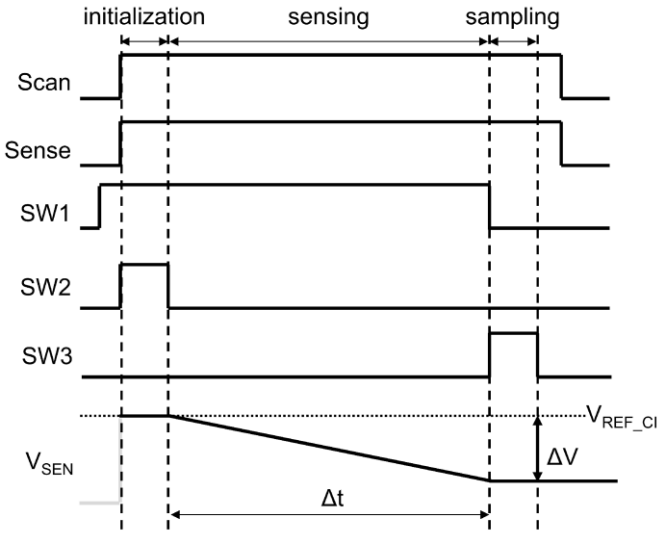

(c)

Fig. 2. (a) 3T1C OLED pixel and simplified block diagram of the proposed sensing circuit. (b) Circuit diagram of a CI amplifier. (c) Timing diagram of the voltage waveforms for the proposed method.

SW1, and SW2 signals are set to a high level. T2 and T3 are then turned on, and V_{DATA} and V_{REF_CI} are applied to the gate and source nodes of T1, respectively. During sensing, SW2 signal is set to a low level, allowing the current to flow to the CI while maintaining the V_{GS} of T1. The input current decreases the output voltage (V_{SEN}) of the CI. During sampling, SW1 signal is set to a low level and SW3 signal is set to a high level, after which the ADC converts the V_{SEN} value to its corresponding digital value. The I_{DS} of T1 is expressed by,

$$I_{DS} = C_{FB}\frac{\Delta V}{\Delta t} \tag{3}$$

where C_{FB} is the capacitance of the feedback capacitor of CI, Δt is the time taken for CI to integrate current, and ΔV is the difference between the V_{REF_CI} and the final V_{SEN}.

V_{TH} and K can be calculated from the corresponding currents in T1 for two different applied voltages (V_{GS1} and V_{GS2}). The currents flowing through T1 can be expressed as shown in (4) and (5).

$$I_{DS1} = K\,(V_{GS1} - V_{TH})^2 \tag{4}$$

$$I_{DS2} = K\,(V_{GS2} - V_{TH})^2 \tag{5}$$

Using (4) and (5), the values of V_{TH} and K can be calculated as shown in (6) and (7).

$$V_{TH} = \frac{V_{GS2}\sqrt{I_{DS1}} - V_{GS1}\sqrt{I_{DS2}}}{\sqrt{I_{DS1}} - \sqrt{I_{DS2}}} \tag{6}$$

$$K = \left(\frac{\sqrt{I_{DS1}} - \sqrt{I_{DS2}}}{V_{GS1} - V_{GS2}}\right)^2 \tag{7}$$

The calculated V_{TH} and K values are added to the V_{DATA} value for compensation. The formula to calculate a new V_{DATA} for compensation is given as follows:

$$V_{DATA\_COMP} = gain \times V_{DATA\_IN} + V_{TH\_CAL} \tag{8}$$

where V_{DATA_COMP} is the new V_{DATA} compensating for V_{TH} and K variations, V_{DATA_IN} is the V_{DATA} determined by original input image data, V_{TH_CAL} is the calculated V_{TH}, and gain is a nonlinear parameter that compensates for the variation of K depending on V_{GS} (i.e., V_{DATA_IN}).

The gain is given as follows:

$$gain = f\left(\sqrt{\frac{1}{K_{CAL}}}, V_{DATA\_IN}\right) \tag{9}$$

where K_{CAL} is the calculated K that is assumed constant for V_{GS1} and V_{GS2}. As shown in (9), the gain is a function of K_{CAL} and V_{DATA_IN}. If K were not dependent on V_{GS}, the gain would be $(K_{CAL})^{-0.5}$. We measured TFTs to get the characteristics of K depending on V_{GS} because K is a non-linear function of V_{GS}. We implemented the nonlinear function expressed by (9) as a look-up table (LUT) based on the measurement results. The adjusted K, K_{ADJ}, is obtained using the (9). Thus, the gain becomes $(K_{ADJ})^{-0.5}$ rather than $(K_{CAL})^{-0.5}$. The calculated values of V_{TH} and K are then added to the V_{DATA} value to compensate for the TFT characteristics, which improves the luminance uniformity of the panel by removing the influence of V_{TH} and K. After the initial variation is sensed and compensated for, the degradation of TFTs is sensed and compensated periodically in vertical blank time using the compensated V_{DATA}. If TFTs degrade during operation, the degradation can be compensated for by

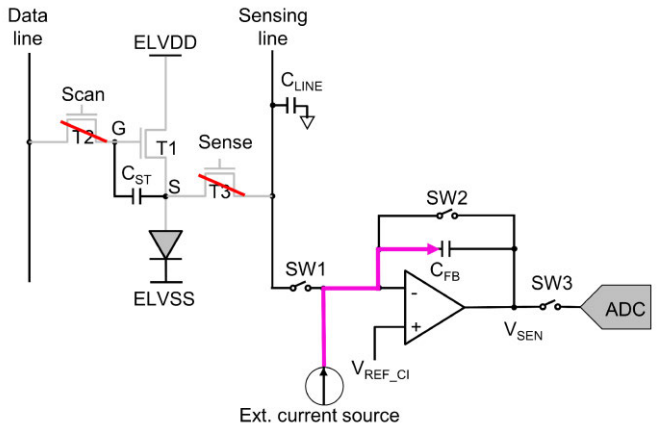

Fig. 3. Schematic diagram of an algorithm to detect the value of C_{FB} by applying a given current through the C_{FB}.

calculating V_{TH} and K in the same way as the first sensing and compensation for the initial variation of TFTs. In this way, our proposed architecture compensates not only for the initial characteristic variation of TFTs but also for their degradation.

III. Sensing Performance Improvement Method

A. How to Compensate for Sensing Circuit Variation

C_{FB}s are manufactured on a silicon wafer. As shown in (3), C_{FB} variation directly affects sensing performance. Thus, it is necessary to overcome the C_{FB} variation. To address this issue, we developed a new algorithm to measure all C_{FB}s.

As shown in Fig. 3, a given current flows through a C_{FB}. Then, we can easily calculate the value of the C_{FB} by measuring V_{SEN} at a given time. In this way, we can find out all C_{FB} values for all CIs. Therefore, we can get all information about all C_{FB}s for all driver ICs and remove the effects of C_{FB} variation.

B. Differential Sensing Method

Accurate sensing of the currents is crucial for perfect compensation of V_{TH} and K. The calculated values of V_{TH} and K are based on the sensed currents. Any errors in the current sensing can result in inaccuracies in the calculation of V_{TH} and K, leading to decreased compensation performance. Several factors can contribute to the decrease in the accuracy of current sensing during I_{DS} sensing, including noise current (i_{NOISE}) from power sources and deviations in current caused by differences in V_{GS} settings [29].

The power supply noise appears as i_{NOISE} in the load capacitance of the sensing line, affecting the I_{DS} during sensing. Additionally, v_{REF_CI}, the noise in V_{REF_CI} generates v_{SEN}, the noise in V_{SEN} as expressed in (10) [30].

$$v_{SEN} = v_{REF\_CI}\left(\frac{C_{LINE}}{C_{FB}} + 1\right) \tag{10}$$

As shown in (10), V_{REF_CI} noise is amplified by the ratio of C_{LINE}/C_{FB}.

A power supply noise commonly affects the entire panel. The current noise at adjacent capacitive loads is usually similar. Thus, we propose a differential sensing method to remove the common i_{NOISE} at the adjacent odd and even lines.

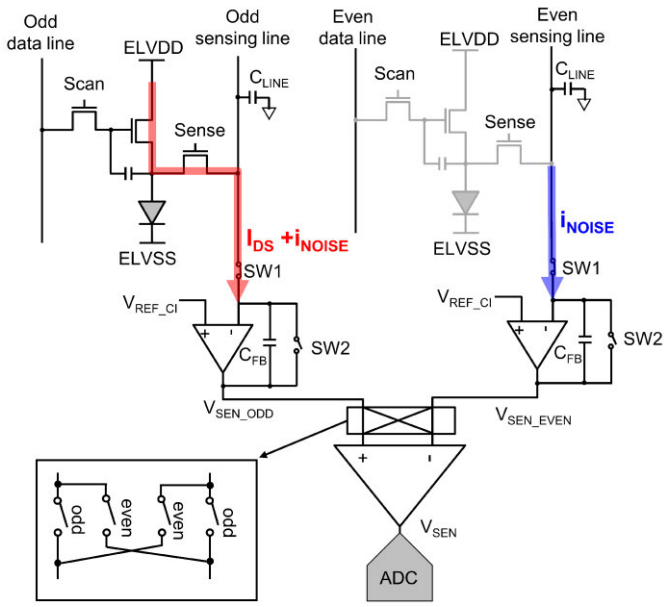

Fig. 4. Simplified block diagram of differential sensing method.

As shown in Fig. 4, this method works by first applying V_{DATA} to the TFTs of the odd line, which causes both I_{DS} and i_{NOISE} to flow. The TFTs on the even line are turned off, resulting in the presence of only i_{NOISE}. As a result, the output voltage of the odd CI, V_{SEN_ODD}, contains both I_{DS} and i_{NOISE}. However, the output voltage of the even CI, V_{SEN_EVEN}, contains only i_{NOISE}. As shown in Fig. 4, the difference amplifier removes the effect of i_{NOISE}, allowing for the accurate, noise-free sensing of I_{DS} by the proposed differential sensing method.

The differential sensing method not only removes the common i_{NOISE} at the adjacent odd and even lines but also the amplified V_{REF_CI} noise. This is because the amplified noises at the odd and even lines are almost identical. By switching the inputs of the difference amplifier, noise-free I_{DS} can be accurately sensed at the even lines. The differential sensing method improves compensation performance by increasing immunity to power supply noises by only sensing TFTs on either odd or even line.

C. Auto-Zero Method

We need to consider offset-induced errors, as the input offset voltages (V_{OS}) of the CIs can result in inaccuracies in current sensing. The deviations in current resulting from differences in the V_{GS} settings can cause errors in the calculation of V_{TH} and K. I_{DS} is dependent on the V_{GS} of T1. Differences in V_{GS} settings can result in deviations in current and inaccuracies in the calculation of V_{TH} and K, even if the TFT characteristics are identical. The offset of the CI results in a difference in the V_S of T1, leading to different V_{GS} settings during initialization. Thus, the offset must be removed during initialization. An auto-zero method can be used to achieve this [31]. The auto-zero method is a technique that samples the offset of the amplifier and then removes it by applying the sampled offset value to the amplifier input.

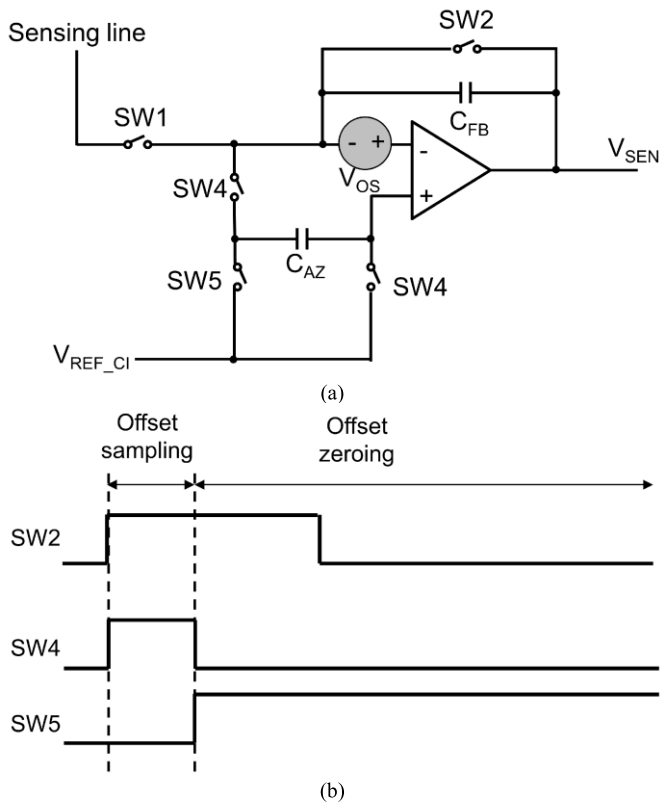

Fig. 5. (a) Simplified block diagram of auto-zero circuit. (b) Timing diagrams of switch signals.

Fig. 5(a) shows the auto-zero circuit, which uses three switches and a capacitor (C_{AZ}) to store the offset. While SW2 is on, auto-zero operates to remove the offset and initialize V_S of T1. Fig. 5(b) shows the waveforms of the switching signals during the auto-zero process, which is performed in two steps: offset sampling and offset zeroing. During offset sampling, SW2 and SW4 signals are set high to store the CI offset voltage in C_{AZ} while SW5 is low. During offset zeroing, only SW4 and SW5 signals are changed to low and high levels, respectively.

The offset voltage stored in C_{AZ} is then added to V_{REF_CI}. By applying $V_{REF\_CI} + V_{OS}$ to the non-inverting input of the CI, the offset voltage is effectively removed.

IV. Simulation Results

We simulated the proposed circuit under ultra-high definition (UHD, 3840 × 2160) resolution and 120 Hz refresh rate conditions using the Smart Simulation Program with Integrated Circuit Emphasis (Smart-SPICE). We simulated using oxide TFTs and white OLEDs (WOLEDs). To compensate for TFT characteristics in real-time, sensing must be completed within the 300 μs vertical blank time. The simulation considered the constraint that the sensing operation could be completed within the time limit, with assumed ΔV_{TH} and ΔK values of ±0.5 V and ±10 %, respectively.

A. Sensing and Compensation

The simulation used V_{DATA} values of 7.2 V and 5.95 V, with V_{REF_CI} of 4.5 V. The Scan and Sense signals had

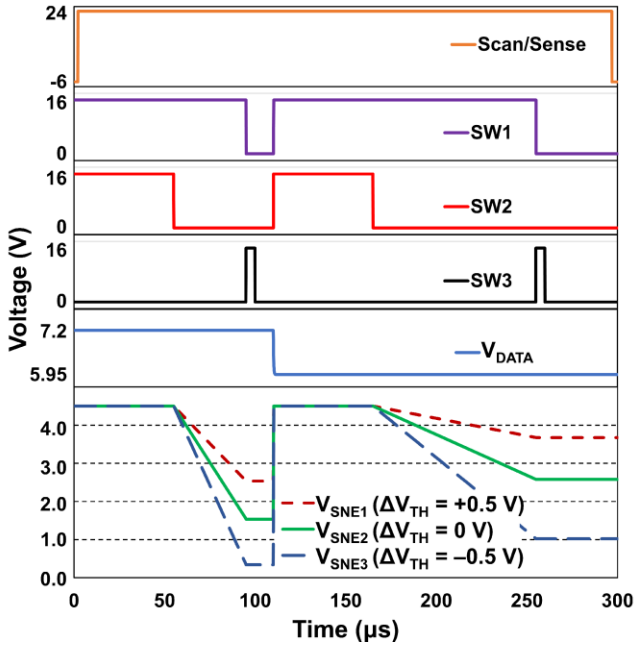

Fig. 6. Simulation results of V_{SEN} depending on three V_{TH} conditions.

positive and negative voltages (V_{GH} and V_{GL}) of 24 V and −6 V, respectively. The supply voltage of the driver ICs was 16 V. The total sensing time, including two initialization times of 2 × 50 μs, was 300 μs. We selected the V_{GS} conditions considering the sensing time and compensation performance. Sensing must be completed within the vertical blank time for real-time compensation. Since we targeted UHD resolution and 120 Hz refresh rate, sensing must be completed within 300 μs. We examined the compensation performance for V_{GS} values that allow sensing within 300 μs and selected the two best V_{GS} values. We compensate by adding the calculated V_{TH} to the V_{DATA} value. Thus, for accurate compensation, the V_{TH} compensation error should be the same as or less than one least significant bit (LSB) of the digital-to-analog converter (DAC) of driver ICs. We determined the V_{REF_CI} voltage level considering the sensing range and resolution. We selected the condition where the sensing range is $\Delta V_{TH} = \pm 0.5$ V or higher, and the resolution is such that ΔV_{TH} is less than one LSB of the DAC. Since the V_{TH} of WOLED is higher than 4.5 V, it did not affect current sensing.

Fig. 6 shows the results of the proposed circuit simulation. As shown in Fig. 6, these results indicate that V_{SEN} reached two different levels for two different current conditions within the 300 μs vertical blank time. The simulation was carried out for three different ΔV_{TH} conditions that resulted in different current values being sensed through the V_{TH} difference.

The simulation was conducted under nine different transistor conditions (T1 to T9) with $\Delta V_{TH} = -0.5$, 0, +0.5 V and $\Delta K = -10$, 0, +10 %.

Table I summarizes the calculated V_{TH} and K values based on the sampled V_{SEN} values for each transistor condition. The initial V_{TH} and K values are represented by ΔV_{TH_I} and K_I, while the calculated values are represented by ΔV_{TH_C} and K_C. The errors in the sensed V_{TH} and K are shown as e_{TH} and e_K, respectively.

TABLE I
CALCULATED V_{TH} AND K DEPENDING ON TRANSISTOR CONDITIONS

	ΔV_{TH_I} (V)	ΔV_{TH_C} (V)	e_{TH} (mV)	K_I (%)	K_C (%)	e_K (%)
T1	0.00	−0.00	−1.7	100	100.1	−0.1
T2	0.00	0.01	7.7	90	89.9	0.1
T3	0.00	−0.01	−6.7	110	109.8	0.2
T4	−0.50	−0.49	7.5	90	89.8	0.2
T5	−0.50	−0.50	0.2	100	99.9	0.1
T6	−0.50	−0.51	−6.2	110	109.9	0.1
T7	0.50	0.51	9.1	90	90.1	−0.1
T8	0.50	0.50	1.5	100	100.2	−0.2
T9	0.50	0.49	−5.3	110	110.2	−0.2

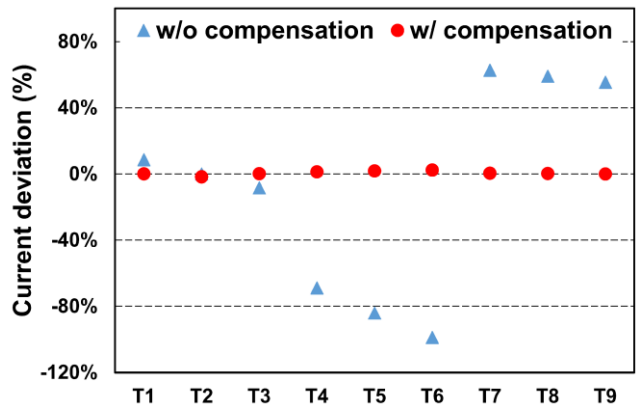

Fig. 7. Current deviations depending on device variations before and after compensation.

The maximum V_{TH} error was 9.1 mV, which is less than one LSB of a 10-bit DAC with a supply voltage of 16 V. The maximum K error was 0.2 %.

Fig. 7 shows the deviation of each TFT's current before and after compensation at 1.45 V of V_{GS} (V_{DATA} = 5.95 V). The current deviation of the TFTs before compensation ranged from −98.8 % to 62.7 %, while after compensation, it ranged from −1.77 % to 2.30 %. After compensation, almost the same current flows through the TFTs, regardless of device variations.

B. Differential Sensing Method

The performance of differential sensing method was evaluated by adding noise to V_{REF_CI} and i_{NOISE}. There are multiple power supplies used to drive an OLED TV panel, such as ELVDD, AVDD, V_{GH}, and V_{GL}. ELVDD supplies emission current to pixels. AVDD is the analog power supply for driver ICs. V_{GH} and V_{GL} are positive and negative power supplies for integrated scan drivers, respectively. For the i_{NOISE} simulation, we superposed the power supply noises except for V_{REF_CI}. The peak-to-peak voltage and frequency of the added noise to

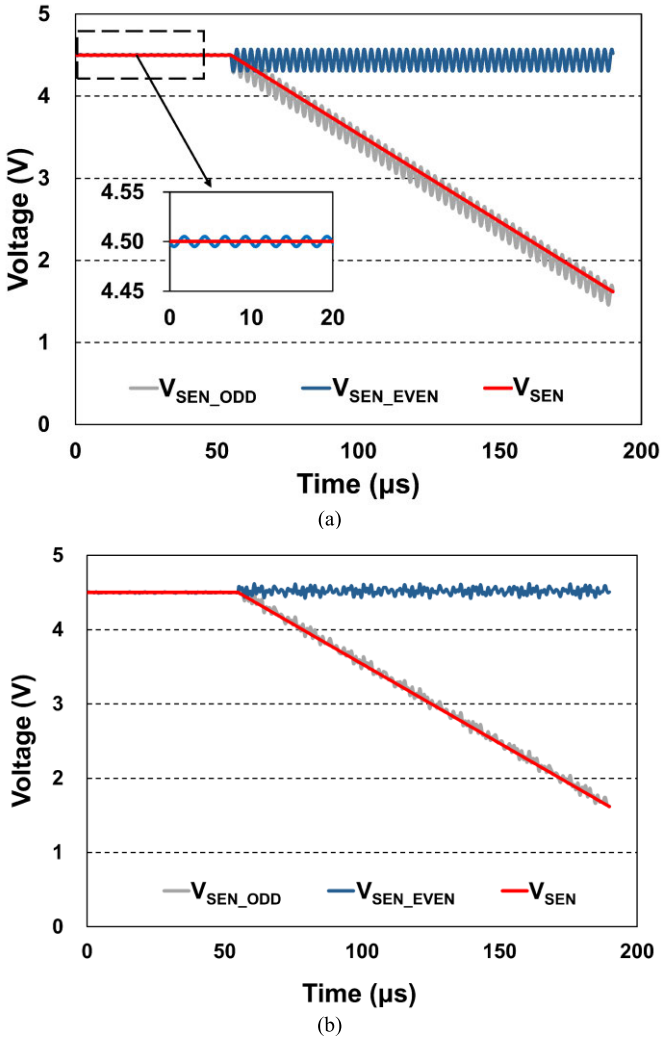

Fig. 8. Sensing error between before and after differential sensing method due to (a) V_{REF_CI} noise and (b) i_{NOISE}.

V_{REF_CI} were set to 10 mV and 400 kHz, respectively. The superposed power supply noise had a peak-to-peak voltage of 20 mV and consists of multiple frequencies. V_{REF_CI} noise and the superposed power supply noise were determined based on measurement data.

Fig. 8 shows differential sensing operation in the case of sensing odd-line TFTs. As shown in Fig. 8(a), V_{REF_CI} noise amplified by the ratio of C_{LINE}/C_{FB} was sensed. This added about 250 mV peak-to-peak noise to V_{SEN_ODD}. As shown in Fig. 8(b), i_{NOISE} was added. This added about 190 mV of peak-to-peak noise to V_{SEN_ODD}. As shown in Fig. 8, V_{REF_CI} noise had a greater influence on sensing than i_{NOISE}. The only noise was sensed in V_{SEN_EVEN}. The noises generated on the odd and even lines were almost identical, so differential sensing method was able to cancel out the noise and only sense the I_{DS}. This demonstrates that differential sensing improves immunity to power supply noise.

C. Auto-Zero Method

Auto-zero is a method that stores the offset voltage of the charge integrator in the C_{AZ}. The stored voltage in C_{AZ} is applied to the non-inverting input of the charge integrator to

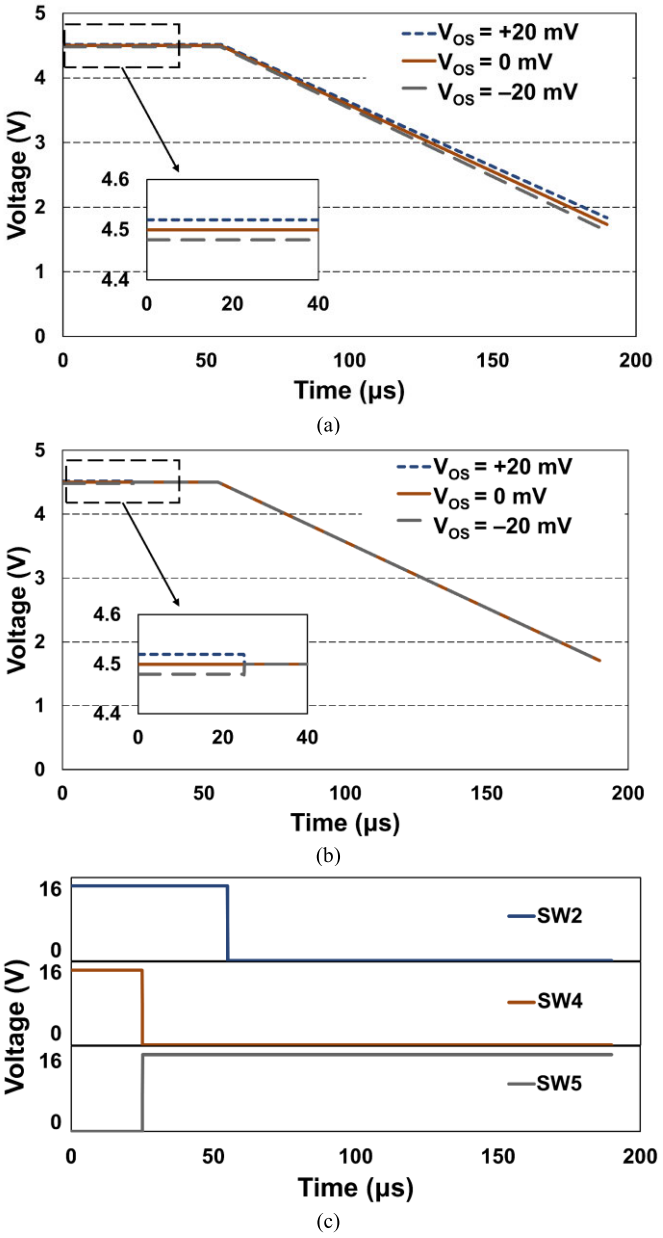

Fig. 9. Simulated V_{SEN} with $V_{OS} = \pm 20$ mV (a) before and (b) after using auto-zero. (c) Timing diagram of control signals for the auto-zero.

remove the offset voltage. Thus, the size of C_{AZ} must be large enough to accurately store the offset voltage while the integrator senses the current of the TFT. However, a larger C_{AZ} will result in a larger chip size. We carefully considered the requirements of auto-zero performance and chip size. We concluded that a C_{AZ} of 1 pF is sufficient to achieve satisfactory auto-zero performance while minimizing the chip size.

Figs. 9(a) and 9(b) show the simulated V_{SEN} waveforms before and after using the auto-zero method, respectively. Fig. 9(c) shows the control signals timing for the auto-zero operation. The offset voltage was set to ± 20 mV to accommodate variations in the IC manufacturing process. The offset sampling step was set to 25 μs to ensure accurate sampling of the CI offset, as shown in Fig. 9(c). As shown in Fig. 9(a), the V_{SEN} values varied depending on the CI offset with a difference of approximately 140 mV. Fig. 9(b) shows

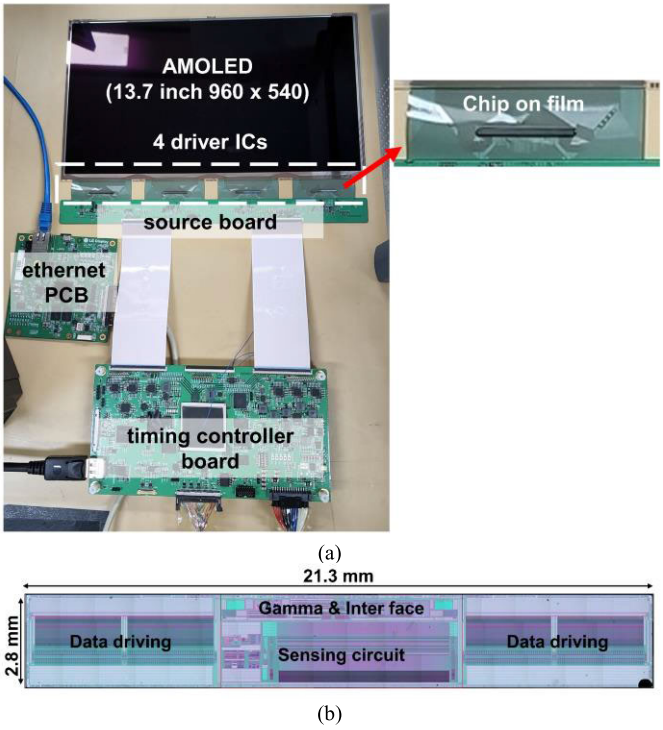

Fig. 10. (a) Photograph of the manufactured display system. (b) Micrograph of a fabricated IC.

that the use of auto-zero effectively reduces the sensing error caused by the CI offset by removing the offset.

V. Measurement Results

The proposed architecture for TFT compensation was verified using a 13.7-inch AMOLED panel with a resolution of 960×540 which has the same pixel density measured in pixels per inch (ppi) as that of a 55-inch UHD display. The panel utilized oxide TFTs and WOLEDs. The driver ICs utilized 10-bit ADCs with a sensing range of 4 V, and the current of red sub-pixels was measured at 1.45 V of V_{GS} ($V_{DATA} = 5.95$ V).

Fig. 10(a) shows a photograph of the manufactured display system, which features a 13.7-inch OLED panel, four driver ICs, a source board, a timing controller board, and a communication board (ethernet PCB).

The driver IC was fabricated using a 0.18 μm CMOS process with 1.8 and 18 V CMOS devices. Fig. 10(b) shows a micrograph of a fabricated IC. The driver IC includes 960 driving channels and 240 sensing channels.

A. Error Reduction Performance

We measured I_{DS} of the driving transistor (T1) in each pixel (a total of 960×540 currents), and collected corresponding digital data converted by the ADC. We proposed the use of differential sensing and auto-zero methods to reduce sensing errors caused by amplifier offset and power supply noise. To evaluate performance of our proposed method, we compared the sensed data before and after using differential sensing and auto-zero method, as shown in Fig. 11.

Fig. 11(a) shows a two-dimensional (2D) map displaying digital current data for all pixels without the application of differential sensing and auto-zero method. The x- and

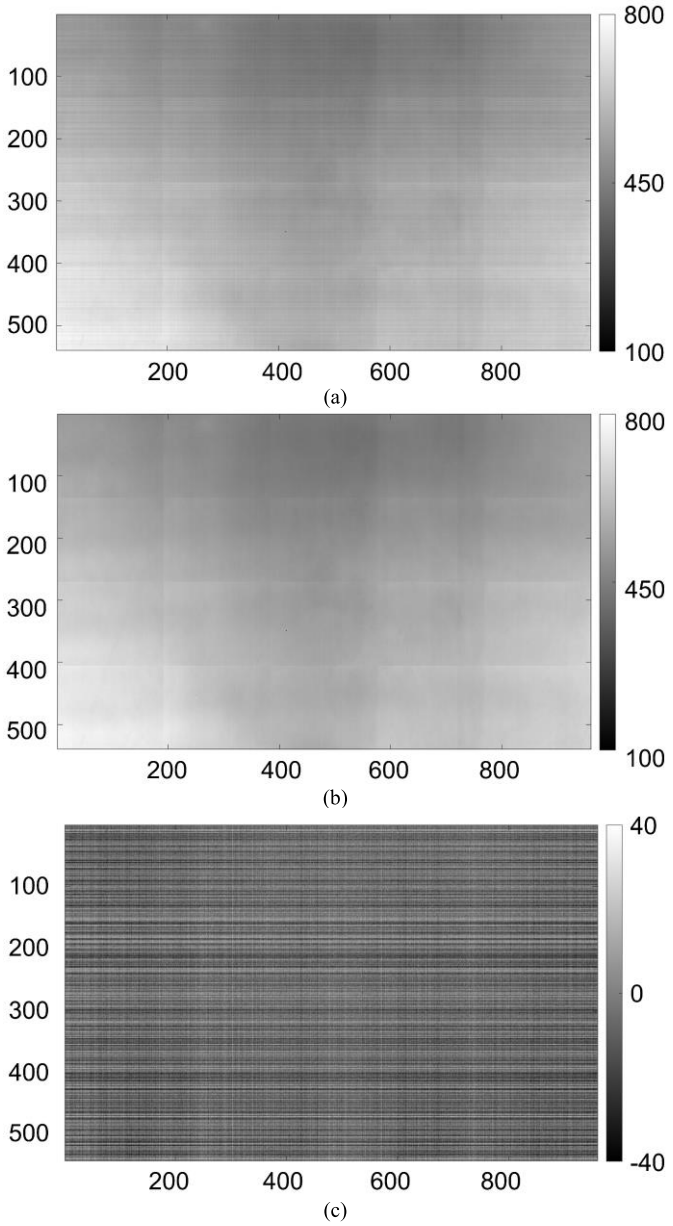

Fig. 11. (a) Sensing map before using differential sensing and auto-zero method. (b) Sensing map after using differential sensing and auto-zero method. (c) Difference between (a) and (b).

y-coordinates represent the measured pixel positions in the horizontal and vertical directions, respectively. This 2D map is referred to as the sensing map. The scale bar on the right side of the sensing map shows the digital values converted by the 10-bit ADC. We can observe horizontal and vertical lines in the sensing map as shown in Fig. 11(a). These horizontal lines were caused by common power supply noise as the TFT currents in a row were sensed simultaneously, while the vertical lines were caused by the CI offset due to the connection of the CIs in the vertical direction. However, after using differential sensing and auto-zero method, the sensing map in Fig. 11(b) shows that most of the horizontal and vertical lines were no longer present. We can expect that compensation performance will be improved as more accurate current sensing is achievable. Fig. 11(c) shows the difference in sensed values before

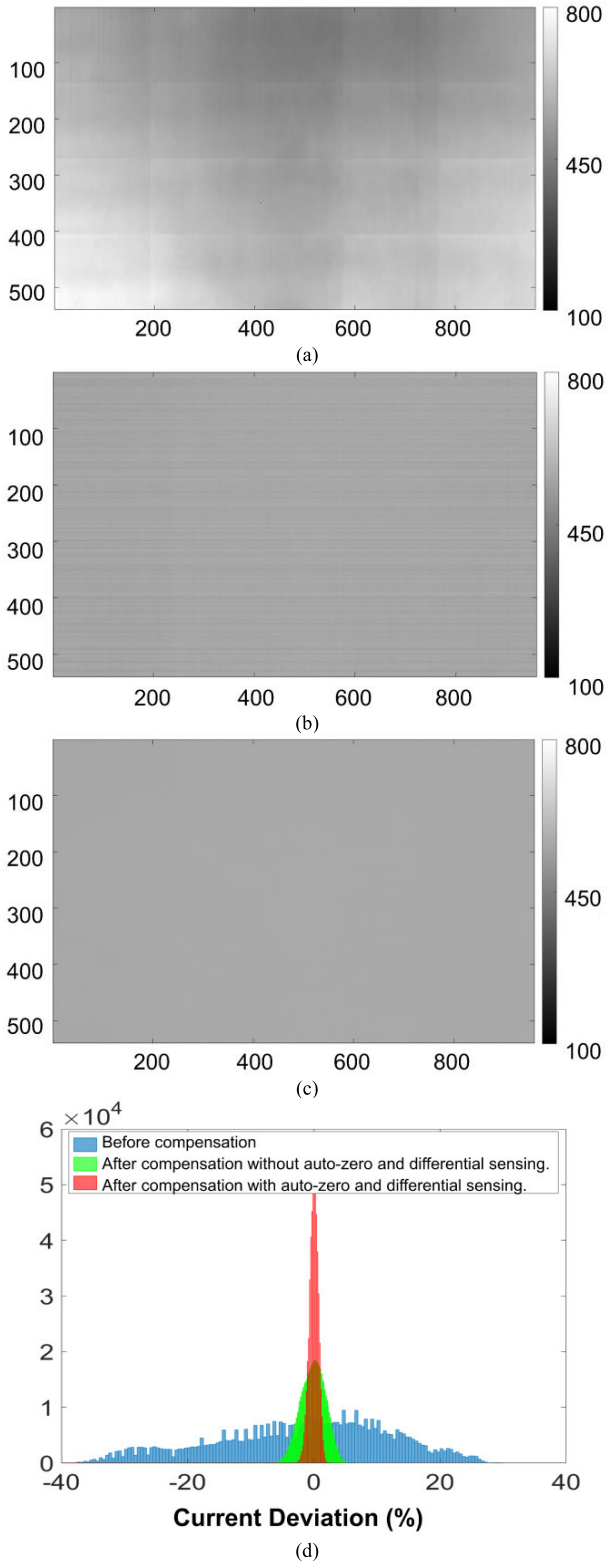

Fig. 12. (a) Sensing map before compensation. (b) Sensing map after compensation without differential sensing and auto-zero method. (c) Sensing map after compensation using differential sensing and auto-zero method. (d) Histogram of current levels for all TFTs in (a), (b), and (c).

and after the use of differential sensing and auto-zero method. The difference was approximately 80 LSB as an ADC value, which represents a sensing error of about 300 mV in terms of the V_{SEN} value.

TABLE II
COMPARISON WITH PREVIOUS WORKS

	This work	Ref [25]	Ref. [27]	Ref. [28]
Pixel structure	3T1C	3T1C	3T1C	3T1C
Sensing method	Current	Voltage	Voltage	Current
Sensing time	300 μs	310 μs (or 610 μs)	1.3 ms	840 μs
V_{TH} shift range	±0.5 V	100 mV	0.5 to 2.5 V	-
K shift range	±10 %	30 %	-	-
V_{TH} max. error	9.1 mV	ΔV_{TH} = 3 mV	ΔV_{TH} = 76.5 mV	-
K max. error	0.2 %	-	-	-
Max. current error with compensation	4.81 %	-	-	6.0 %

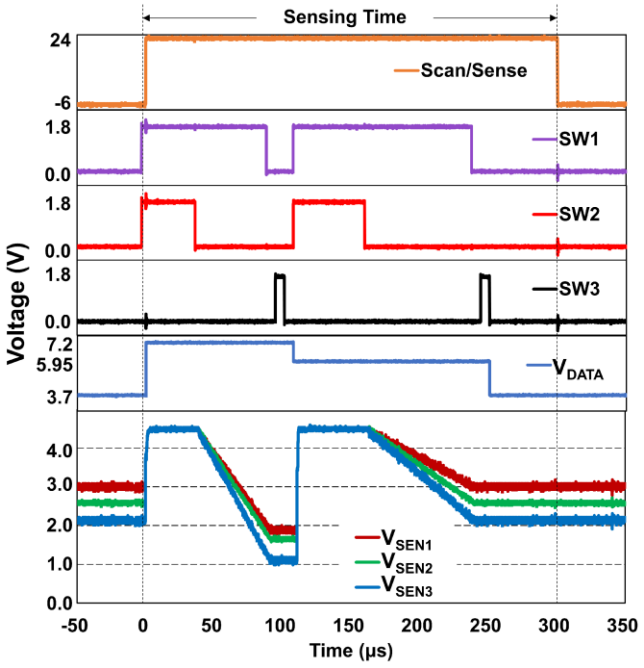

Fig. 13. The measured waveform of control signals for sensing and V_{SEN}.

B. Compensation Performance

Fig. 12(a) shows the sensing map before compensation. The center of the panel appears the darkest, indicating the lowest current levels. On the other hand, the lower-left area was the brightest, indicating the highest current levels. Fig. 12(b) shows the sensing map after compensation without differential sensing and auto-zero method. There are horizontal and vertical lines caused by power supply noise and amplifiers' offsets. Fig. 12(c) shows the sensing map after compensation using differential sensing and auto-zero method, demonstrating that almost the same current values were sensed at all pixels after compensation. Fig. 12(d) shows the histogram of the measured current levels before and after compensation. The obtained ΔV_{TH} and ΔK values in the manufactured 13.7-inch panel were −0.28 V to 0.24 V and −3 % to +2 %, respectively. The current deviation before compensation ranged from −40.44 % to +29.69 %. After compensation without differential sensing and auto-zero method, the current deviation ranged from −6.83 % to +7.01 %. Although the mura of the panel has been significantly reduced, there was still a current deviation due to noise, as shown in Fig. 12(b). After compensation using differential sensing and auto-zero method, the current deviation ranged from −2.65 % to +2.16 %.

The reported threshold luminance value for a mura with an irregular shape was approximately 7.4 % [32]. Thus, it can be confirmed that the compensation has been effective.

Fig. 13 shows the measured waveforms of the control signals for sensing and V_{SEN}. The SW1 to SW3 outputs of the timing controller were 1.8 V signals, while the other signals were the same as the simulation conditions. As shown in Fig. 13, the V_{SEN} completed the sensing operation for different current conditions within 300 μs. This confirms that TFT characteristics can be compensated in real-time under the UHD resolution and 120Hz refresh rate conditions.

In a display with a 120Hz refresh rate, it is possible to sense even or odd pixels of one horizontal line every 1/120 second. Thus, in a WRGB pixel structure where four sub-pixels share one sensing line, it is possible to compensate for TFT characteristics in real-time every 144 seconds (1/120 × 2160 × 4 × 2) for OLED products with UHD resolution. Here, a refresh time of 1/120 s indicates the frame time at which the image is updated, while 2160 represents the number of row lines in the display. The number 4 refers to the number of sub-pixels used to create each pixel (WRGB), and 2 indicates the differential sensing (even or odd pixel).

Fig. 14(a) shows a photograph of the panel before compensation, and as previously discussed, the center of the panel had a dark mura. It is apparent that the sensing map shown in Fig. 12(a) and the panel photograph in Fig. 14(a)

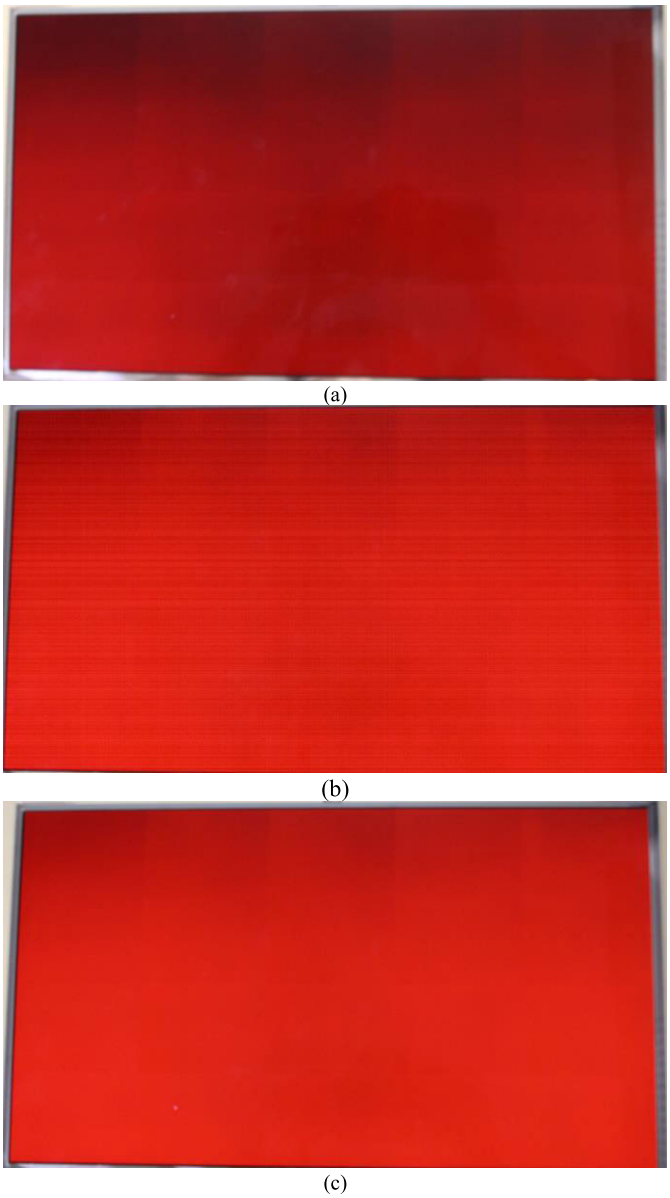

Fig. 14. Photographs of OLED panel adopting (a) no compensation (b) compensation without differential sensing and auto-zero method (c) compensation using differential sensing and auto-zero method.

exhibit strong similarities. Fig. 14(b) shows a photograph of the panel after compensation without differential sensing and auto-zero method. The mura in the panel has significantly reduced, but we can observe horizontal and vertical lines. The horizontal and vertical lines shown in Fig. 14(b) are very similar to Fig. 12(b). Fig. 14(c) shows a photograph of the panel after compensation using differential sensing and auto-zero method, which resulted in a significant reduction of the noise. The proposed method successfully compensated for TFT characteristics, as demonstrated by the luminance uniformity. We have demonstrated that the TFT characteristics in a 13.7-inch AMOLED display panel can be successfully compensated using external compensation circuits incorporating CI, along with the utilization of differential sensing and auto-zero methods. The proposed compensation approach effectively reduced sensing errors caused by amplifier offset and power supply noise, resulting in improved luminance uniformity and mura reduction, as shown in Fig. 14(c).

Table II summarizes the performance of the proposed external compensation compared to that proposed in previous studies on real-time TFT compensation. Previous studies took more than 300 μs for sensing time and only compensated for V_{TH} without considering the change in K. In contrast, the proposed external compensation method can compensate for both V_{TH} and K within 300 μs. Thus, the proposed method is superior to the previous studies in terms of both sensing time and compensation performance.

VI. Conclusion

In this paper, we have proposed a novel real-time external compensation method that uses CI to reduce sensing times and compensate for TFT characteristics. By utilizing two different sensed currents, V_{TH} and K can be accurately calculated. A new technology to measure all feedback capacitors of all CIs has been proposed to improve sensing performance. By using differential sensing and auto-zero, we successfully reduce the sensing errors and improve the compensation performance. The performance of the proposed sensing and compensation approaches was verified using a 13.7-inch AMOLED panel. As the sensing can be completed within 300 μs, which is the vertical blank time for UHD resolution and 120 Hz refresh rate, the proposed method can compensate for TFT characteristics in real-time. Therefore, the proposed sensing and compensation method is an effective solution for high-resolution and large-sized OLED display applications.

References

[1] H. J. Jang, J. Y. Lee, G. W. Baek, J. Kwak, and J.-H. Park, "Progress in the development of the display performance of AR, VR, QLED and OLED devices in recent years," *J. Inf. Display*, vol. 23, no. 1, pp. 1–17, Feb. 2022, doi: 10.1080/15980316.2022.2035835.

[2] C. H. Oh, H. J. Shin, W. J. Nam, B. C. Ahn, S. Y. Cha, and S. D. Yeo, "21.1: Invited paper: Technological progress and commercialization of OLED TV," in *SID Symp. Dig. Tech. Papers*, vol. 44, no. 1. Vancouver, BC, Canada, 2013, pp. 239–242.

[3] H. J. Jang, J. Y. Lee, J. Kim, J. Kwak, and J.-H. Park, "Progress of display performances: AR, VR, QLED, and OLED," *J. Inf. Display*, vol. 21, no. 1, pp. 1–9, Feb. 2020, doi: 10.1080/15980316.2020.1720835.

[4] C. W. Tang and S. A. VanSlyke, "Organic electroluminescent diodes," *Appl. Phys. Lett.*, vol. 51, no. 12, pp. 913–915, Sep. 1987, doi: 10.1063/1.98799.

[5] M. Stewart, R. S. Howell, L. Pires, and M. K. Hatalis, "Polysilicon TFT technology for active matrix OLED displays," *IEEE Trans. Electron Devices*, vol. 48, no. 5, pp. 845–851, May 2001, doi: 10.1109/16.918227.

[6] A. Nathan, A. Kumar, K. Sakariya, P. Servati, S. Sambandan, and D. Striakhilev, "Amorphous silicon thin film transistor circuit integration for organic LED displays on glass and plastic," *IEEE J. Solid-State Circuits*, vol. 39, no. 9, pp. 1477–1486, Sep. 2004, doi: 10.1109/JSSC.2004.829373.

[7] S. Lee, Y. Chen, J. Kim, H. Kim, and J. Jang, "Transparent AMOLED display driven by split oxide TFT backplane," *J. Soc. Inf. Display*, vol. 26, no. 3, pp. 164–168, Apr. 2018, doi: 10.1002/jsid.646.

[8] D. U. Jin et al., "65.2: *Distinguishedpaper*: World-largest (6.5') flexible full color top emission AMOLED display plastic film its bending properties," in *SID Symp. Dig. Tech. Papers*, vol. 40, no. 1. San Antonio, TX, USA, 2009, pp. 983–985.

[9] H. Yamaguchi et al., "74.2 L: Late-news paper: 11.7-inch flexible AMOLED display driven by a-IGZO TFTs on plastic substrate," in *SID Symp. Dig. Tech. Papers*, vol. 43, no. 1. Boston, MA, USA, 2012, pp. 1002–1005.

[10] Y. G. Mo et al., "Amorphous-oxide TFT backplane for large-sized AMOLED TVs," *J. Soc. Inf. Disp.*, vol. 19, no. 1, pp. 16–20, Jun. 2011, doi: 10.1889/JSID19.1.16.
[11] G. R. Chaji et al., "Electrical compensation of OLED luminance degradation," *IEEE Electron Device Lett.*, vol. 28, no. 12, pp. 1108–1110, Dec. 2007, doi: 10.1109/LED.2007.909854.
[12] D. W. Park et al., "53.5: High-speed AMOLED pixel circuit and driving scheme," in *SID Symp. Dig. Tech. Papers*, vol. 41, no. 1. Seattle, IL, USA, 2010, pp. 806–809.
[13] C.-L. Lin et al., "Compensation pixel circuit to improve image quality for mobile AMOLED displays," *IEEE J. Solid-State Circuits*, vol. 54, no. 2, pp. 489–500, Feb. 2019, doi: 10.1109/JSSC.2018.2881922.
[14] T. Hasumi, S. Takasugi, K. Kanoh, and Y. Kobayashi, "46.2: New OLED pixel circuit and driving method to suppress threshold voltage shift of a-Si:H TFT," in *SID Symp. Dig. Tech. Papers*, vol. 37, no. 1. San Francisco, CA, USA, 2006, pp. 1547–1550.
[15] J. S. Yoon et al., "58.2: 55-inch OLED TV using optimal driving method for large-size panel based on InGaZnO TFTs," in *SID Symp. Dig. Tech. Papers*, vol. 45, no. 1. San Diego, CA, USA, 2014, pp. 849–852.
[16] J. Koh, K. Kang, C. Shin, S.-Y. Lee, and S. Yoon, "Compensating nonuniform OLED pixel brightness in a vertical blanking interval by learning TFT characteristics," *IEEE Trans. Electron Devices*, vol. 68, no. 7, pp. 3396–3402, Jul. 2021, doi: 10.1109/TED.2021.3079232.
[17] H.-J. In et al., "An advanced external compensation system for active matrix organic light-emitting diode displays with poly-Si thin-film transistor backplane," *IEEE Trans. Electron Devices*, vol. 57, no. 11, pp. 3012–3019, Nov. 2010, doi: 10.1109/TED.2010.2067750.
[18] H.-J. In and O.-K. Kwon, "External compensation of nonuniform electrical characteristics of thin-film transistors and degradation of OLED devices in AMOLED displays," *IEEE Electron Device Lett.*, vol. 30, no. 4, pp. 377–379, Apr. 2009, doi: 10.1109/LED.2009.2014885.
[19] Y.-H. Tai and C.-H. Lin, "An external compensation method for AMOLED using the concept of ramp-stop: A novel external compensation method for AMOLED," *J. Soc. Inf. Display*, vol. 25, no. 11, pp. 672–675, Nov. 2017, doi: 10.1002/jsid.616.
[20] H. J. Shin et al., "7.1: Invited paper: Novel OLED display technologies for large-size UHD OLED TVs," in *SID Symp. Dig. Tech. Papers*, vol. 46, no. 1. San Jose, CA, USA, 2015, pp. 53–56.
[21] H. J. Shin et al., "50.1: Invited paper: Technological progress of panel design and compensation methods for large-size UHD OLED TVs," in *SID Symp. Dig. Tech. Papers*, vol. 45, no. 1. San Diego, CA, USA, 2014, pp. 720–723.
[22] T. G. Kim et al., "50.3: A novel power saving technology for OLED TV with external TFT compensation," in *SID Symp. Dig. Tech. Papers*, vol. 45, no. 1. San Diego, CA, USA, 2014, pp. 728–731.
[23] R. Tani et al., "64.2: Panel and circuit designs for the world's first 65-inch UHD OLED TV," in *SID Symp. Dig. Tech. Papers*, vol. 46, no. 1. San Jose, CA, USA, 2015, pp. 950–953.
[24] J. Fu et al., "16-3: A fast TFT threshold voltage sensing method based on iterative feedback," in *SID Symp. Dig. Tech. Papers*, vol. 48, no. 1, May 2017, pp. 204–206.
[25] K.-S. Kang, J.-K. Lee, J.-M. Kang, and S.-Y. Lee, "A novel real-time TFT threshold voltage compensation method for AM-OLED using double sampling of source node voltage," *IEEE J. Electron Devices Soc.*, vol. 9, pp. 311–317, Feb. 2021, doi: 10.1109/JEDS.2021.3058348.
[26] S. Takasugi et al., "Advanced compensation technologies for large-sized UHD OLED TVs," *J. Soc. Inf. Display*, vol. 24, no. 7, pp. 410–418, May 2016, doi: 10.1002/jsid.442.
[27] Y.-F. Jin and H.-J. Xie, "P-1.8: External compensation for TFT Vth&mobility using linear charge sense method in AMOLED display," in *SID Symp. Dig. Tech. Papers*, vol. 49. Los Angeles, CA, USA, 2018, pp. 541–543.
[28] H.-C. Seol, J.-H. Ra, S.-K. Hong, and O.-K. Kwon, "An AMOLED panel test system using universal data driver ICs for various pixel structures," *IEEE Trans. Electron Devices*, vol. 64, no. 1, pp. 189–194, Jan. 2017, doi: 10.1109/TED.2016.2627561.
[29] J.-S. Bang et al., "A hybrid AMOLED driver IC for real-time TFT nonuniformity compensation," *IEEE J. Solid-State Circuits*, vol. 51, no. 4, pp. 966–978, Apr. 2016, doi: 10.1109/JSSC.2015.2504416.
[30] T. J. Mego, "Dc current measurements," in *Atomic, Molecular, and Optical Physics: Charged Particles*, vol. 29. Cambridge, MA, USA: Academic, 1995, pp. 421–435.
[31] C. C. Enz and G. C. Temes, "Circuit techniques for reducing the effects of op-amp imperfections: Autozeroing, correlated double sampling, and chopper stabilization," *Proc. IEEE*, vol. 84, no. 11, pp. 1584–1614, Nov. 1996, doi: 10.1109/5.542410.
[32] K. Lim et al., "P.42: Estimation and evaluation of image sticking on OLED device," in *SID Symp. Dig. Tech. Papers*, vol. 44, no. 1. Vancouver, BC, Canada, 2013, pp. 1152–1154.

Myung Gi Lim received the B.S. degree in electrical engineering from Myong Ji University, Yongin, South Korea, in 2011. He is currently pursuing the Ph.D. degree with the Department of Information Display, Kyung Hee University, Seoul, South Korea. He is a Senior Research Engineer with LG Display, Seoul.

Seung-Woo Lee (Senior Member, IEEE) received the B.S., M.S., and Ph.D. degrees in electrical engineering from the Korea Advanced Institute of Science and Technology in 1993, 1995, and 2000, respectively, where he conducted research on integrated driver circuits for poly-Si TFT-LCDs. He joined Samsung in 2000, where his work has focused on the development of key driving technologies for active-matrix liquid-crystal displays. He has played a key role in image quality enhancement, high-end LCD timing-controller design, FPGA evaluation of new driving schemes, next-generation LCD interface technologies, and advanced LCD driving schemes for large-size TV applications. He was also in charge of the development of analog-digital mixed-signal ICs for TFT-LCDs. He joined Kyung Hee University, Seoul, South Korea, where he has been studying novel display systems and visual perception. He is currently a Full Professor with the Department of Information Display, Kyung Hee University. He has been active as a Senior Member of the Society for Information Display since 2010. He was a recipient of the 2008 Chester Sall Award from the IEEE Consumer Electronics Society in 2010.